

## Near space radiation dosimetry in Australian outback using a balloon borne energy compensated PIN diode detector

Bhaskar Mukherjee<sup>a, b, \*</sup>, Xiaofeng Wu<sup>c</sup>, Tomasz Maczka<sup>d</sup>, Trevor Kwan<sup>c</sup>, Yijun Huang<sup>c</sup>, Vladimir Mares<sup>d</sup>

<sup>a</sup>School of Physics (A28), The University of Sydney, NSW 2006, Australia

<sup>b</sup>Detector and Sensor Group, West German Proton Therapy Centre Essen (WPE), Hufeland Strasse 55, 45147 Essen, Germany

<sup>c</sup>School of Aerospace, Mechanical and Mechatronics Engineering, The University of Sydney, NSW 2006, Australia

<sup>d</sup>Helmholtz Zentrum München, Institute of Radiation Protection, Ingolstädter Landstraße 1, 85758 Neuherberg, Germany

### Abstract

This paper reports the near space ballooning experiment carried out at Australian outback town West Wyalong (33°51'S, 147°24'E) on 19 July 2015. Several dedicated electronic detectors including digital temperature and acceleration (vibration) sensors and an energy compensated PIN-diode gamma ray dosimeter were installed in a thermally insulated Styrofoam payload box. A 9V Lithium-Polymer battery powered all the devices. The payload box was attached to a helium-filled latex weather balloon and set afloat. The balloon reached a peak burst altitude of 30 km and then soft-landed aided by a self-deploying parachute 66.2 km away from the launch site. The payload box was retrieved and data collected from the electronic sensors analysed. The integrated cosmic ray induced photon ambient dose equivalent recorded by the PIN diode detector was evaluated to be  $0.41 \pm 0.06 \mu\text{Sv}$ . Furthermore, a high-altitude extended version of commercially available aviation dosimetry package EPCARD.Net (**E**uropean **P**rogram package for the **C**alculation of **A**viation **R**oute **D**oses) was used to calculate the ambient dose equivalents during the balloon flight. The radiation environment originated from the secondary cosmic ray shower is composed of neutrons, protons, electrons, muons, pions and photons. The photon ambient dose equivalent estimated by the EPCARD.Net code found to be  $0.47 \pm 0.09 \mu\text{Sv}$ . The important aspects of balloon based near-space radiation dosimetry are highlighted in this paper.

### Keywords

Australian outback; Cosmic ray shower; EPCARD.Net; High-Altitude Balloon Mission; Pfozter-Maximum; PIN-diode dosimeter

---

\*Corresponding Author: Tel: +61 0458 505378; Email: bhamukh@gmail.com

## 1. Introduction

The advent of modern scientific ballooning facilitated the scientific communities worldwide to carry out high quality scientific research in the fields of atmospheric science, space weather studies, heliophysics, remote sensing and telecommunication research (**Gaskin et al., 2014**). Furthermore, the availability of low cost latex weather balloons and electronic components as well as open source information technology facilitated students and researchers of educational institutions to participate in cutting edge scientific endeavours (**Gai et al., 2014**).

The upper atmosphere is constantly bombarded with very high-energy particles from outer space known as galactic cosmic rays (GCR). The GCR on the other hand, interacts with air molecules producing secondary cosmic radiation, predominantly made of high-energy neutrons, electrons as well as muons, pions and protons and gamma rays (**Wissmann, 2006**). Evidently, GCR influences the space weather and inflicts detrimental radiological effects on high-altitude aviation crews and frequent flying passengers (**Jones et al., 2005**). Studies on cosmic radiation in the upper atmosphere using high-altitude balloons are highlighted in recent literature (**Iyudin et al., 2015**).

Under the framework of space education activities at the School of Aerospace, Mechanical and Mechatronics Engineering (SAMME) of the University of Sydney we have focussed on the following important research projects (a) Development radiation detectors and electronic instrumentations using COTS (Commercially Off The Shelf) components for ongoing high-altitude ballooning and future student picosatellite missions (**Bouweester and Guo, 2010, Stein, 2014**). (b) Near-space cosmic ray dosimetry and subsequent high-altitude extension of the well-known EPCARD.Net software application originally developed for aircrew dosimetry (**Mares et al., 2009**). This paper highlights the high-altitude ballooning mission carried out at Australian outback town West Wyalong (33°51'S, 147°24'E) on 19 July 2015.

## 2. Materials and Methods

### *2.1 Near Space Ballooning Mission*

A commercially available low cost latex weather balloon filled with helium gas was utilised as the carrier. A thermally insulated Styrofoam container (external dimension: 35 cm × 35 cm × 35 cm, wall thickness: 5.0 cm) was used as payload box. The payload box housed a high-resolution miniature video camera and a GPS module with integrated 900 MHz ultra long-range radio modem connected to an instrumentation board. The board was interfaced to the following electronic instruments made of COTS components:

(a) External and internal temperature sensors, (b) A digital accelerometer and (c) An energy compensated PIN diode based gamma ray dosimeter. A high-capacity 9V Lithium-polymer battery powered the instruments. The material properties of the balloon, parachute and payload box are summarised in **Table 1**. A pictorial description of the ballooning mission including photo shots taken by the miniature video camera is depicted in **Figure 1**. The architecture of the balloon borne instrumentation board is shown in **Figure 2**. The construction principle of the PIN-diode based gamma ray dosimeter (this work) is depicted in **Figure 3**. The photon (gamma rays) mass energy attenuation coefficients of SiO<sub>2</sub> (building material of the PIN-diode) and Lead (material of energy compensation filter) (**Hubble and Seltzer, 1993**) are shown as functions photon energy in **Figure 4**.

The payload box (total weight: 1.8 kg) was tethered to the helium-filled latex balloon (**Figure 1a**) and set afloat (09:14 EST). The balloon reached a peak burst altitude of 30 km and subsequently landed (11:37 EST) 66.2 km away from the launch site aided by a self-deploying parachute. The balloon flight co-ordinates were continuously recorded by the GPS module and transmitted to ground station via the radio modem (**Figure 5**). All balloon flight data including gamma dosimeter counts were recorded in real-time and stored in the SD card located in the electronic instrumentation board (**Figure 2**).

## 2.2 Electronic Instrumentation Board

The electronic instrumentation board (**Figure 2**) was made of a custom designed printed circuit board (PCB) (Dimension: 100 mm × 100 mm × 2 mm) incorporating the following components (i) *Microcontroller unit (MCU)*: The MCU embodies a low voltage (1.8 V to 3.6 V) Mixed Signal Microcontroller with ultra low power consumption (Model: MSP430F551x, Manufacturer: Texas Instruments; USA). A low power watchdog-timer (WDT) (Model: MAX6814, Manufacturer: Maxim Integrated Products, San Jose, USA;) augments MCU operation. (ii) *Data storage and power supply*: A standard SD card reader (SDC) with a 32 GB card integrated to MCU was used to store data generated by the instruments during the mission. A heavy-duty (10000 mAh) 9V lithium polymer battery (LPB) used as power supply. (iii) *GPS and Radio modem*: A high-resolution GPS module (Model: MAX-M8, Manufacturer: uBlox; USA) with an integrated miniature Quad-V antenna contentiously recorded the balloon coordinates (latitude, longitude and altitude) and stored in the SD card. Furthermore, the coordinates were transmitted to ground station using the 900 MHz ultra long-range radio modem (TCV) (Model: RFD900, Manufacturer: RFDesign Pty Ltd, Sumner Park, QLD 4074, Australia).

(iv) *Temperature detectors*: Pairs of high precision (12-bit), low power consuming digital thermometer chip (Model: DS1731, Manufacturer: Maxim Integrated Products, San Jose, USA) operating within the temperature range (-55 °C to +125 °C) were used as internal (IT) and external (ET) temperature sensors. The internal (IT) and external (ET) sensor chip was attached to the instrumentation board and outer wall of the payload box respectively. (v) *Acceleration (vibration) detector*: A 3-axis ultra low power, high-resolution (12-bit) Digital Accelerometer chip (Model: ADXL345, Manufacturer: Analog Devices, Norwood, USA) was firmly attached (soldered) to the instrumentation board. The ADXL345 chip is capable to assess acceleration level up to 16 G and operates flawlessly within the temperature range (-40 °C to +85 °C). (vi) *Gamma radiation dosimeter*. The authors had developed a sensitive gamma dosimeter to measure the cosmic gamma radiation during balloon flight using a commercially available PIN-diode module RD2014 (**Teviso, 2015**) (discussed in detail in the following sections).

### 2.3 Principle of PIN-diode

The Silicon PIN junction diodes (**Holm-Siedle and Adams, 2002**) are now widely used in various scientific and engineering applications including radiation detection and monitoring tasks at high-energy physics experiments (**Ravotti et al., 2008**). The principle of PIN diode (**Holland, 1989**) is depicted in **Figure 1a**. The PIN diode is constructed on a thin wafer of high-purity silicon dioxide (SiO<sub>2</sub>), which is an insulator. In the PIN diode the acceptor (P) zone (1) is formed at one end of the bulk, and the donor (N) zone (2) at other, by doping with boron (B) and phosphorus (P) atoms respectively. Subsequently, a depletion region, or equivalently, the intrinsic (I) zone (3) is formed between P and N zones. The end terminals (5, 6) of the diode are connected to the bias voltage supply. The  $\gamma$ -rays impinging on the depletion region generate a current (I) proportional to gamma dose rate.

### 2.4 PIN-diode Gamma Ray Dosimeter

The authors have used the commercially available PIN diode gamma radiation sensor RD2014 developed by Teviso Sensor Technology (**Teviso, 2015**) to build the gamma dosimeter. The RD2014 embodies the following subsystems: (i) An array of Si-PIN diodes, (ii) Low noise amplifier, (iii) Comparator circuit, (iv) Threshold-Reference circuit and (v) TTL output stage. The above components are housed in a robust Electro-Magnetic-Interference (EMI) shielded enclosure (28mm×16mm×5mm). The operating bias across the PIN-diode detector was kept fixed at 4.5 V by the manufacturer and not controllable externally. The dosimeter calibration factor relevant to <sup>60</sup>Co gamma rays (E<sub>av</sub> = 1.25 MeV) was also set at a fixed value (5.8 cpm/μSv.h<sup>-1</sup> ± 15%) by the manufacturer.

The dosimeter output was interfaced to a pulse shaping circuit (PSC) based on a QUAD 2-input NOR Gate chip HCF4001 B (Manufacturer: ST Microelectronics, Tucson, USA). The output pulse rate from the dosimeter module depends only on impinging gamma dose rate. It is worthwhile to note that the NOR gate chip was used purely as a pulse shaping entity, having no influence on pulse rate amplification, i.e. the dosimeter calibration factor (**Spieler 2005**). The principle of the SUGAR (Sydney University Gamma Ray) dosimeter is shown in **Figure 3b**.

#### 2.4 Compensation of Gamma Energy Dependence

Si-PIN diodes are highly sensitive to low energy photons (gamma rays) as shown in the plot (**Figure 4**) of mass energy attenuation coefficient ( $\mu_{en}/\rho$ ) of SiO<sub>2</sub> as a function of photon energy (**Hubble and Seltzer, 1993**). In order to achieve the energy-independent response of the PIN-diode based SUGAR dosimeter the authors had implemented a novel filter technique described elsewhere (**Olsher and Eisen, 1996**). This energy compensation method is now widely used in many commercially available PIN-diode based gamma area monitors with a broad energy response. As a suitable energy compensation filter the authors have selected commercially available lead foil of 0.2 mm thickness (**Pradhan and Bhatt, 1979**). The RD2014 Dosimeter module was thoroughly wrapped with 0.2 mm thick lead foil (**Figure 3c**) The mass energy attenuation coefficient ( $\mu_{en}/\rho$ ) of Lead as a function of photon energy (**Hubble and Seltzer, 1993**) is depicted in **Figure 4**.

This implicates the complete cut-off of the low energy photons and validates a gamma energy-independent (flat) response of the PIN-diode based SUGAR dosimeter.

#### 2.5 Effect of High-Energy Electrons

A PIN-diode detector is also sensitive to beta rays (electrons). The beta energy spectra of a myriad of radioisotopes starting from the lowest (<sup>3</sup>H,  $E_\beta = 5.72$  keV) to highest (<sup>106</sup>Rh,  $E_\beta = 1.425$  MeV) average emission energy are presented elsewhere (**Cross, et al., 1983**). On the other hand, the electrons prevalent at the balloon altitude (30 km) are originated from cosmic ray showers possessing energies up to 100 MeV (**Mares et al., 2009**). The PIN-diode (SUGAR) dosimeter response to high-energy electrons ( $R_{HEE}$ ) is directly proportional to number of electrons stopped (absorbed) in the diode and is defined as:

$$R_{HEE} = r_0(I_0 - I_t)/I_0 \quad (1)$$

Where,  $r_0$ ,  $I_0$  and  $I_t$  stand for PIN-diode response to radio-isotopic beta rays (**Cross et al. 1983**), high-energy electron (balloon altitude) fluence at entrance and exit surfaces of the dosimeter respectively. Further:

$$I_t = I_0 \exp(-\mu_m x_t \rho) \quad (2)$$

Where,  $\mu_m$  ( $\text{cm}^2 \text{mg}^{-1}$ ),  $x_t$  (0.05 cm) and  $\rho$  ( $2320 \text{ mgcm}^{-3}$ ) stand for mass energy attenuation coefficient of electrons in  $\text{SiO}_2$  (**Gürler and Yalçin, 2005, Gupta and Gupta, 1980**), thickness of the  $\text{SiO}_2$  wafer (**Figure 3c**) and density of  $\text{SiO}_2$  respectively. Further:

$$\mu_m = 0.008Z^{0.28}E_m^{-[1.57-(Z/160)]} \quad (3)$$

Where,  $Z$  (10.8) and  $E_m$  (100 MeV) stand for the effective atomic number of  $\text{SiO}_2$  (**Figure 4**) and maximum electron energy at balloon altitude (**Mares et al. 2009**) respectively.

By substituting the numerical values of  $Z$  and  $E_m$  in equation 3 the value of  $\mu_m$  was calculated to be  $1.54 \times 10^{-5}$  ( $\text{cm}^2 \text{mg}^{-1}$ ). By substituting the numerical values of  $\mu_m$ ,  $x_t$  and  $\rho$  in equation 2 the value of  $I_t$  was calculated to be  $0.998I_0$

Finally, by substituting the value of  $I_t$  in equation 1 the response of PIN-diode based SUGAR dosimeter to 100 MeV electrons ( $R_{\text{HEE}}$ ) was evaluated to be  $0.0018r_0$

This validates that the PIN-diode based SUGAR dosimeter is insensitive to high-energy electrons from cosmic ray shower at balloon altitude (this work).

#### 2.4 Verification of Calibration factor

The dose rate calibration constant ( $5.8 \text{ cpm}/\mu\text{Svh}^{-1} \pm 15\%$ ) of RD2014 gamma sensor as given by the manufacturer was verified using a  $^{60}\text{Co}$  ( $E_G = 1.25 \text{ MeV}$ ) gamma check source as follows: The SUGAR dosimeter was attached to a calibrated Pocket Alarm Dosimeter (PAD) (Model: RAD-51/60, Manufacturer Rados Technology Oy, Turku, Finland). Like SUGAR dosimeter the RAD-51/60 was also based on energy compensated Si PIN-diode. The data output line of the dosimeter (**Figure 3b**) was connected to a digital storage oscilloscope (Model: USB-RedScope, Manufacturer: Meilhaus Elektronik GmbH, Puchheim, Germany). A  $370 \text{ MBq}$  ( $10 \text{ mCi}$ )  $^{60}\text{Co}$  gamma source was brought to proximity of the dosimeters. The PAD showed a dose rate of  $250 \mu\text{Svh}^{-1}$ . The pulse train displayed by the oscilloscope was saved and shown in **Figure 6**. After the verification of calibration factor the SUGAR dosimeter was permanently mounted (soldered) on the instrumentation board (**Figure 2**).

Gamma dose rate calibration factor ( $k$ ) given by the manufacturer was verified using the pulse count rate of SUGAR dosimeter exposed to gamma rays from a  $^{60}\text{Co}$  ( $E_G = 1.25 \text{ MeV}$ ) source.

$$k = 60c/D_G \quad (1)$$

Where,  $c$  ( $23 \text{ pulses.s}^{-1}$ ) and  $D_G$  ( $270 \mu\text{Sv.h}^{-1}$ ) represent the pulse count rate (**Figure 6**) and  $^{60}\text{Co}$  gamma exposure rate respectively. By substituting the values of  $c$  and  $D_G$  in equation 1 the value of  $k$  evaluated to be  $5.1 \text{ cpm}/\mu\text{Svh}^{-1}$ . Evidently, the evaluated value of dose rate

calibration constant (k) found to be very close to value given by the manufacturer ( $5.8 \text{ cpm}/\mu\text{Svh}^{-1} \pm 15\%$ ).

The implementation of energy-compensation filter (**Olsher and Eisen, 1996, Pradhan and Bhatt, 1979**) using 0.2 mm thick Lead foil cuts off the influence of low-energy gammas thereby making the SUGAR dosimeter practically gamma energy independent. Hence, the study of energy dependence of the SUGAR dosimeter using MVp x-ray beams (bremsstrahlung) becomes redundant.

### 3. Results and Data Analysis

#### 3.1 Data collected during Balloon flight

After retrieval of the payload box the SD card from the electronic instrumentation board (**Figure 2**) was removed and saved data downloaded in a MS Excel spreadsheet. Evidently, all data sets of interest i.e., GPS coordinates, internal and external temperatures, acceleration and SUGAR dosimeter counts were recorded as functions of time starting from balloon release. For further analysis the following data sets were expressed explicitly as functions of elapsed time: **(a)** Acceleration and balloon altitude (GPS) versus elapsed time (**Figure 7**). **(b)** Internal and external temperatures and balloon altitude (GPS) versus elapsed time (**Figure 8**), **(c)** SUGAR dosimeter counts and balloon altitude (GPS) versus elapsed time (**Figure 9**).

#### 3.2 Data Analysis

During the flight the ultra-long-range radio modem transmitted the GPS coordinates of the balloon in real-time to data receiving station situated in a 4-Wheel drive vehicle. Guided by the GPS ground trace our team retrieved the balloon at the location 62 km east of the launching spot (**Figure 5**).

The acceleration (vibration) and altitude profiles (**Figure 7**) elucidate the movement characteristics of the balloon flight: **(a)** A sharp acceleration spike ( $\sim 1.5\text{G}$ ) occurred after the balloon release. **(b)** Balloon steadily reached peak altitude (30 km) in 7500s at an ascending rate of  $4.0 \text{ ms}^{-1}$  without suffering significant acceleration ( $\sim 1\text{G}$ ). **(c)** Balloon ruptured at burst altitude (30 km) resulting in large acceleration spike ( $\sim 2 \text{ G}$ ). The payload camera took the photo shot of the balloon burst showing latex fragments flying apart (**Figure 1c**). **(d)** Payload box started its free fall at a descending rate of  $25 \text{ ms}^{-1}$  thereby underwent indiscriminate accelerations ( $\sim 2 \text{ G}$ ). The parachute opened at the altitude approx. 1 km resulting in a “slowed down” free fall. The payload box finally hit the ground 1100 s after the balloon burst (**Figure 1c**) with an acceleration of  $\sim 1.5 \text{ G}$  at impact on ground.

The temperature and altitude profiles (**Figure 8**) revealed a steady fall of temperature measured outside the payload box ( $T_{out}$ ) until the balloon reached burst altitude (30 km). The temperature began to rise sharply while the payload box started its free fall and evidently attained ambient level after it soft-landed. On the other hand, the temperature recorded inside the payload box ( $T_{in}$ ) remained almost steady, dropped from 285 K to 270 K during the entire balloon flight. This justified the high thermal insulating efficacy of the Styrofoam payload box (**Table 1**).

The accumulated counts from the SUGAR dosimeter and the balloon altitude are depicted in **Figure 9** as functions of elapsed time. The integrated ambient photon dose equivalent  $H^*_G(10)$  during the balloon mission was calculated as follows:

$$H^*_G(10) \mu\text{Sv} = (60N/tTk) \times (T/3600) \quad (2)$$

Where, N (1420 counts), t (10s), T (8580 s), k ( $5.1 \text{ cpm}/\mu\text{Svh}^{-1}$ ) represent the accumulated SUGAR dosimeter counts (**Figure 9**), dosimeter sampling time, duration of the balloon mission and dosimeter calibration factor (equation 1) respectively. By substituting above numerical values in equation 2 the integrated photon ambient dose equivalent was calculated to be  $0.36 \mu\text{Sv}$ .

The first derivative (count rate) of the accumulated photon counts (**Figure 9**) was evaluated using the MS Excel spreadsheet and multiplied with the SUGAR dosimeter calibration constant  $5.1 \text{ cpm}/\mu\text{Svh}^{-1}$  to obtain the photon ambient dose equivalent rate  $\dot{H}^*_G(10)$ . The photon ambient dose equivalent rate and balloon altitude as functions of elapsed time are presented in **Figure 10**. The results identified the regions of Pfozter-Maximum (**Carlson and Watson, 2014**) during the ascending (PM1) and descending (PM2) phases of the balloon. The integrated photon ambient dose equivalent accumulated during the balloon mission was calculated to be  $0.36 \pm 0.05 \mu\text{Sv}$ .

#### 4. Radiation Exposure Calculation with EPCARD.Net

The EPCARD.Net (**Mares et al., 2009**) constitutes the latest version of the EPCARD (European Program package for the Calculation of Aviation Route Doses) program that was approved for official use for dose assessment of radiation exposure due to secondary cosmic radiation at aviation altitudes by the German Aviation Authority (LBA). Moreover, EPCARD was validated by on board measurements of commercial passenger flights (**Lindborg et al., 2004**) where an agreement between measured and calculated doses better than  $\pm 20\%$  was demonstrated. The EPCARD solution is based on the results of extensive Monte Carlo (MC)

calculations (**Roesler et al., 2002**) taking into account all physical processes that govern the interaction of cosmic radiation with air molecules in the upper Earth's atmosphere, using well-known FLUKA Monte-Carlo code (**Ferrari et al., 2005**). Using a NASA model of primary cosmic rays impinging upon the top of the atmosphere (Badhwar, 1997), the secondary particle spectra of neutrons, protons, photons, electrons and positrons, muons, and pions were calculated for 36 heights above sea level from ground level to the top of the atmosphere (i.e. for altitudes from 0.3 to 49.5 km) for all possible physical circumstances of solar activity and geomagnetic shielding conditions. To take into account the most recent data of geomagnetic shielding, EPCARD.Net uses data on the geomagnetic field for current epoch, calculated by the MAGNETOCOSMICS code (Desorgher, 2006) developed at the University of Bern by the Cosmic Ray Group (Bütikofer, 2007). The solar potential is derived from the continuously operating NM's. Since 2010, data from the Cosmic Ray Station of Sodankylä Geophysical Observatory (Oulu unit) has been used (Kananen, 1991).

The EPCARD.Net code bestows an advanced version of the previous EPCARD program ver. 3.34 (**Schraube et al., 2002**) giving more accurate results in calculation of ambient dose equivalent  $H^*(10)$ . A set of fluence-to-dose conversion coefficients for the respective particle type from the FLUKA calculations (Pellicioni, 2000) is employed, to calculate ambient dose equivalent,  $H^*(10)$ , and effective dose,  $E$ , separately for each particle type. The EPCARD.Net database includes energy-averaged dose conversion coefficients calculated by folding each single particle fluence spectrum with the appropriate dose conversion function (Mares, 2004; Mares 2007), which depend on barometric altitude, cut-off rigidity, and solar activity, because the shape of the particle energy spectra depends also on these parameters. Typically, the code requires the following input data: **(a)** Date of flight, **(b)** Take-off and landing times, **(c)** Geographical coordinates of take-off and landing points, **(d)** Flight route with waypoints (including longitude, latitude and altitude).

The average cruising altitude for long haul flights by civilian aircrafts worldwide ranges from 30,000 to 40,000 feet (9 - 12 km), which is below the Pfozter-Maximum. With the increasing penetrating depth in the atmosphere, the fluence rate of the entering primary particles (protons) drops, whereas the fluence rate of secondary particles increases and reaches its maximum at an altitude of around 20 km, known as Pfozter-Maximum after German Physicist Georg Pfozter (1909-1981). The altitude of the Pfozter-Maximum depends on solar activity and latitude (**Carlson and Watson, 2014**).

Hence, in order to simulate the cosmic radiation exposure relevant to high-altitude balloon mission scenarios the authors (VM, TM) have extended the upper limit of the officially

approved EPCARD.Net code to 30 km, according MC calculations of Roesler et al., (2002). The input data including the balloon launch date (19 July 2015), time of launch (09:15 EST Australia), time of landing (11:30 EST Australia), geographical location (West Wyalong: 33°51'S, 147°24'E) and altitude versus time profile (GPS data) was delivered to high-altitude extended EPCARD.Net code. The ambient dose equivalents  $H^*(10)$  relevant to all major cosmic ray components, i.e. neutrons, electrons, protons, photons, muons and pions were explicitly calculated. The results are presented in **Table 3** and graphically depicted in **Figures 11** and **Figure 12**.

## 5. Summaries and Conclusion

This report highlights the second educational high-altitude ballooning (HAB) mission carried out by the School of Aerospace, Mechanical and Mechatronics Engineering of the University of Sydney in Australian outback town West Wyalong. We have designed and tested various electronic sensors based on COTS components, performed high-altitude photography and developed the GPS based tracking and radio communications systems.

One of the main goals of this project was the cosmic ray dosimetry at high-altitude using a balloon borne PIN diode detector SUGAR (Sydney University GAMMA RAY) dosimeter developed by one of the authors (BM). The secondary cosmic ray is composed of a myriad of particles including neutrons, electrons, protons, photons, muons and pions, whereas the SUGAR dosimeter is predominantly sensitive to photons. Hence, we have used the EPCARD.Net code to simulate the ambient dose equivalents relevant to all individual components of the cosmic ray explicitly (**Table 3**). The photon ambient dose equivalent measured by the SUGAR dosimeter (0.36  $\mu\text{Sv}$ ) agreed well with the same of the cosmic ray photon (0.47  $\mu\text{Sv}$ ) estimated by EPCARD.Net code (**Figure 11d**). Nevertheless, it is about 30% lower than that calculated with EPCARD.Net due to cut-off of photon contribution below approximately 0.3 MeV (see Fig. 4). In contrast to SUGAR the EPCARD.Net takes the whole energy range of secondary cosmic-ray photons ( $E > 0.2$  keV) into account.

The upper limit (25 km) of the ambient dose equivalent estimation of the EPCARD.Net code originally developed for commercial aviation dosimetry was extended to 30 km in order to facilitate its usage in high altitude (near space) dosimetry related tasks.

The dynamic response of the SUGAR dosimeter was found to be fast enough to identify the regions of Pfozter-Maximum encountered by the balloon during ascending (4.0  $\text{m}\cdot\text{s}^{-1}$ ) and descending (25.0  $\text{m}\cdot\text{s}^{-1}$ ) phases (**Figure 10**). The dosimeter also endured the violent peaks of acceleration (vibrations) experienced during various stages of the balloon flight (**Figure 7**).

Evidently, by utilising the value of photon ambient dose equivalent rate recorded by the SUGAR dosimeter in conjunction with the simulation data from EPCARD.Net code one can parameterise the ambient dose equivalents arising from all other cosmic ray components, i.e. neutrons, protons, electrons, muons and pions (**Figure 12b**). These experimental results could be useful to develop a lightweight and cost-effective personal dosimeter for aircrew and frequent flyers.

## **6. Acknowledgements**

The authors would like to thank the dedicated team of graduate students of School of Aerospace, Mechanical and Mechatronics Engineering (SAMME) of the University of Sydney for actively cooperating during the ballooning mission and Professor Dr. Rod Cross of School of Physics, the University of Sydney for critical review of the manuscript.

## 7. References

- Badhwar, G. D. The radiation environment in low-Earth orbit. *Radiat. Res.* 148, 3–10, (1997).
- Bouweester, J., Guo, J. 2010. Survey of worldwide pico and nanosatellites missions, distributions and subsystem technology. *Acta Astronautica* **67**, 854-862.
- Bütikofer, R., Flückiger, E.O. and Desorgher, L. Characteristics of near real-time cutoff calculations on a local and global scale, 30th International Cosmic Ray Conference, Mérida, México (2007).
- Carlson, P., Watson, A.A. 2014. Erich Regener and the ionisation maximum of the atmosphere. *Hist. Geo. Space Sci.* **5**, 175-182.
- Cross, WG., Ing, H., Freedman, N. 1983. A short atlas of beta-ray spectra. *Phys. Med. Biol.* **28**, 1251-1260.
- Desorgher, L., 2006. MAGNETOCOSMICS: Geant 4 Application for Simulating the Propagation of Cosmic Rays Through the Earth's Magnetosphere. University of Bern, <http://cosray.unibe.ch/~laurent/magnetocosmics/>
- Ferrari, A., Sala, P.R., Fasso, A., Ranft, J. 2005. FLUKA: A Multi Particle Transport Code - 386, Geneva, Switzerland, CERN, INFN, SLAC.
- Gai, M., Guglieri, G., Lattanzi, M.G., Lombardi, A., Mana, M., Masserano, L., Musso, I., Navone, P. 2014. A scientific mission based on a high altitude stratospheric balloon. *Int. Jour. Aerospace Sci.* **3**(1), 18-29.
- Gaskin, J.A., Smith, I.S., Jones, W.V. 2014. Introduction to the special issue on scientific balloon capabilities and instrumentation. *Jour. Astron. Instr.* **3**(2), 1-18.
- Gupta, SK., Gupta, DK. 1980. Continuous slowing-down approximation range of 50 keV-100 MeV electrons. *J. Appl. Phys.* **52**(3), 1175-1178.
- Gürler, O., Yalçın, S. 2005. A practical method for calculation of mass-attenuation coefficients of  $\beta$  particles. *Annals of Nuclear Energy* **32**, 1818-1925.
- Holland, S. 1989. Fabrication of detectors and transistors on high-receptivity silicon. *Nucl. Instr. Meth.* **A275**, 537-541.
- Holm-Siedle, A., Adams, L. 2002. *Handbook of Radiation Effects*, 2<sup>nd</sup> Edition, Oxford University Press, UK.

- Hubble, J.H., Seltzer, S.M. 1993. Tables of X-ray mass attenuation coefficients and mass energy absorption coefficients from 1 keV – 20 MeV for elements  $Z = 1$  to 92 and 48 additional substances of dosimetric interest. *Radiat. Res.* **136**, 147-170.
- Iyudin, A.F., Bogomolov, V.V., Galkin, V.I., Golovanov, I.A., Krasnov, A., Markelova, A.K., Markelov, I., Morgunova, Y., Oseldo, M.I., Panasyuk, M.I., Rozhkov, G., Svertilov, S.I. 2015. Instruments to study fast neutrons fluxes in upper atmosphere with the use of high-altitude balloons. *Adv. Space Res.* **56**, 2073-2079.
- Kananen, H., P.J. Tanskanen, L.C. Gentile, M.A. Shea and D.F. Smart, A quarter of a century of relativistic solar cosmic ray events recorded by the Oulu neutron monitor, *Proc. 22nd ICRC*, 3, 145-148, 1991.
- Lindborg, L., Bartlett, D., Beck, P., McAulay, I., Schnuer, K., Schraube, G., Spurny, F. 2004. EURADOS. Cosmic Radiation Exposure of Aircraft Crew: Compilation of Measured and Calculated Data. Luxembourg, Belgium, European Commission, Office for Official Publication of the European Communities. 1-271.
- Mares, V., Roesler, S. and Schraube, H.: Averaged particle dose conversion factors in air crew dosimetry. *Radiat. Prot. Dosim.* 110, 1-4 , 2004, pp. 371-376
- Mares, V. and Leuthold, G., Altitude-dependent dose conversion coefficients in EPCARD. *Radiat. Prot. Dosim.* 126(1-4), 581-584 (2007).
- Mares, V., Maczka, T., Leuthold, G., Rühm, W. 2009. Aircrew dosimetry with a new version EPCARD. *Radiat. Prot. Dosim.* **136**, 262-266.
- Olsher, R.H., Eisen, Y. 1996. A filter technique for optimising the photon energy response of a silicon PIN-diode dosimeter. *Radiat. Prot. Dosim.* **67**, 271-279.
- Pelliccioni, M. Overview of fluence-to-effective dose and fluence-to-ambient dose equivalent conversion coefficients for high energy radiation calculated using FLUKA code. *Radiat. Prot. Dosim.* 88(4), 279–297 (2000).
- Pradhan, A.S., Bhatt, R.C. 1979. Metal filters for the compensation of photon energy dependence of the response of  $\text{CaSO}_4$ : Dy-Teflon TLD discs. *Nucl. Instr. Meth.* **166**, 497-501.
- Ravotti, F., Glaser, M., Moll, M., Saigne´, F. 2008. BPW34 commercial p-i-n diodes for high-level 1-MeV neutron equivalent fluence monitoring. *IEEE Trans. Nucl. Sc.* **55**(4), 2133-2140.

- Roesler, S., Heinrich, W. and Schraube, H. 2002. Monte Carlo calculation of the radiation field at aircraft altitudes. *Radiat. Prot. Dosim.* **98**(4), 367-388.
- Schraube, H., Leuthold, G., Heinrich, W., Roesler, S., Mares, V. and Schraube, G. 2002. EPCARD – European program package for the calculation of aviation route doses, User's manual. GSF-National Research Center, Neuherberg, Germany (2002). ISSN 0721 - 1694. GSF-Report 08/02
- Spieler, H. 2005. *Semiconductor Detector Systems*, Oxford University Press, UK.
- Stein, T.A. 2014. CubeSat-ready Radiation Monitor Front-Electronics. The 6<sup>th</sup> European CubeSat Symposium, Estavayer-Lac, Switzerland, October 14-17.
- Teviso 2015. *Product (Sensors) Instruction Manual*, Teviso Sensor Technologies, Bern, Switzerland.
- Wissmann, F. 2006. Long-term measurements of  $H^*(10)$  at aviation altitudes in the northern hemisphere. *Radiat. Prot. Dosim.* **121**(4), 347-357.

## Figures and Tables

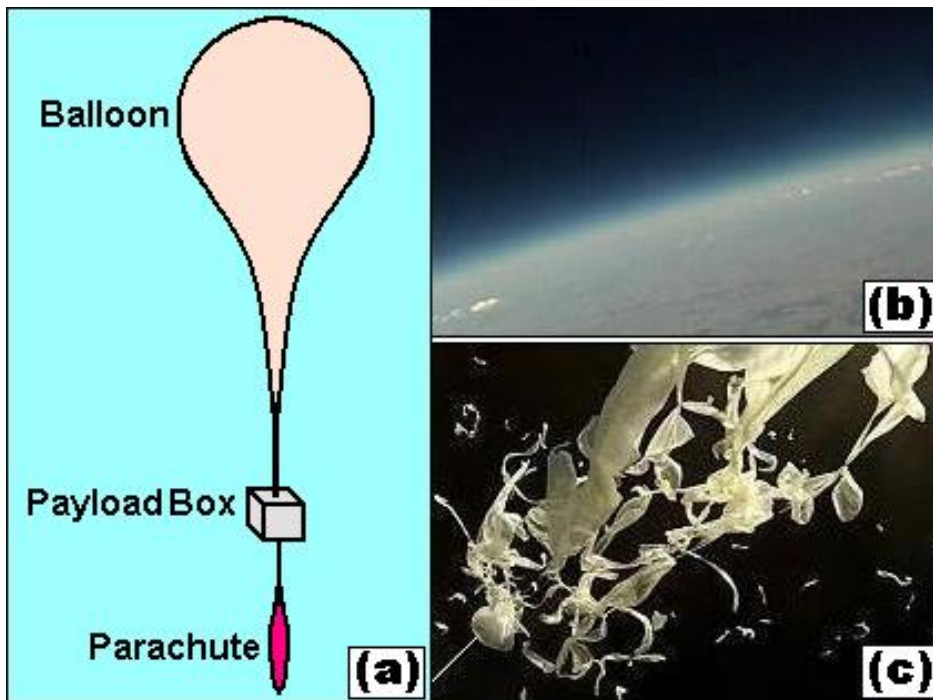


**Figure 1:** (a) The major subsystems of the ballooning mission including the balloon, payload box and parachute. (b) Screen-shot of the sky taken at high altitude; curvature of the earth is clearly visible. (c) Screen-shot of the balloon-burst took place at an altitude of 30 km, balloon fragments were flying apart and brightly illuminated by sunlight; whereas the sky in background remained pitch black.

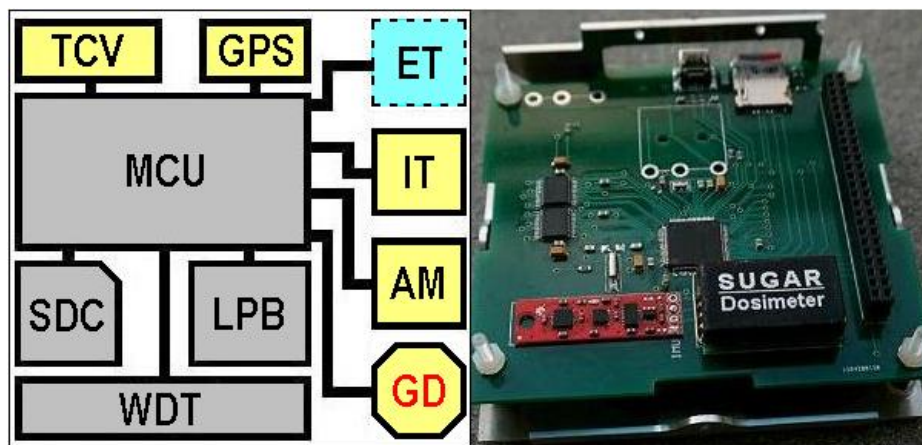


**Figure 2:** Depicting the architecture of the balloon borne instrumentation board incorporating: Micro Controller Unit (MCU), 32 GB SD Card with reader (SDC), Watchdog with timer (WDT), 9V Lithium Polymer Battery (LPB), 900 MHz Ultra long range radio modem (TCV), Global Positioning System module (GPS), External temperature sensor (ET), Internal temperature sensor (IT), Digital accelerometer (AM), Energy compensated Gamma ray (SUGAR) dosimeter (GD) (Left) and a photograph of the prototype board (Right).

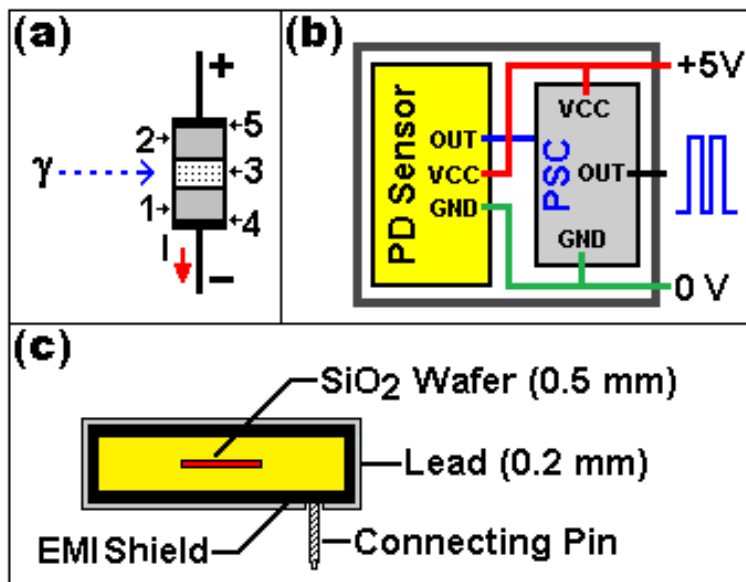


**Figure 3:** (a) Schematic diagram depicting the principle of PIN diode. (b) Schematic diagram of the SUGAR (Sydney University GAMMA Ray) dosimeter showing the PIN-Diode sensor module interfaced to pulse shaping circuit (PSC). (c) Cross section of the PIN diode dosimeter module highlighting the SiO<sub>2</sub> wafer, Electromagnetic Interference (EMI) shield and the energy compensation filter made of 0.2 mm thick Lead foil.

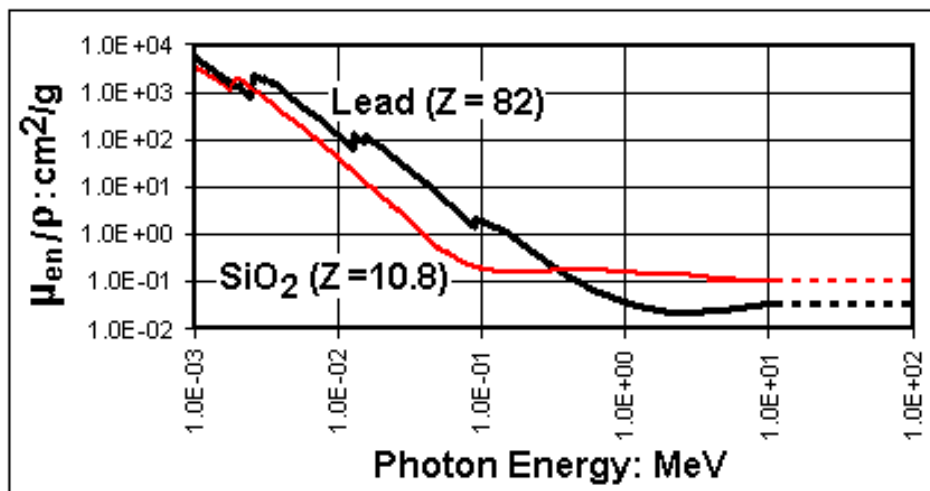


**Figure 4:** Photon mass energy absorption coefficients (Hubble and Seltzer, 1993) of commercial Lead ( $\rho = 11.34 \text{ gcm}^{-3}$ ) and SiO<sub>2</sub> ( $\rho = 2.32 \text{ gcm}^{-3}$ ) are plotted as functions of photon energy



**Figure 5:** Showing the GPS ground trace of the balloon flight. The traversed distance between the launching (West Wyalong) and landing (Weddin Mountains National Park) locations was 66.2 km.

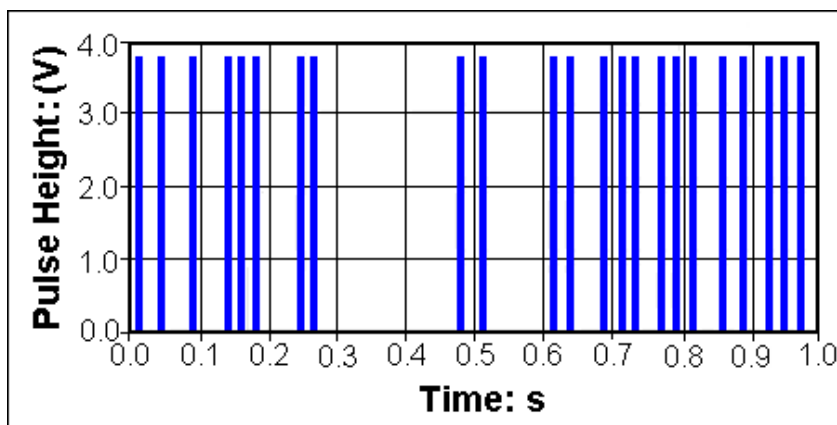


**Figure 6:** Output pulse train from SUGAR dosimeter recorded with a digital storage oscilloscope corresponds to a pulse height and a width of 3.8 V (TTL) and 10 ms respectively during  $^{60}\text{Co}$  irradiation.

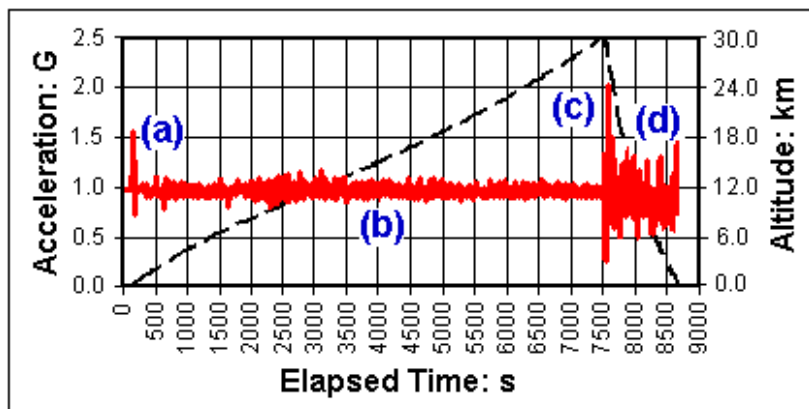


**Figure 7:** Acceleration (vibration) profile recorded by on board digital accelerometer and balloon altitude as functions of elapsed time. The average ascending rate of the balloon and the descending rate of the payload box were calculated to be  $4.0$  and  $25.0 \text{ ms}^{-1}$ , respectively. The maximum acceleration (vibration) endured by the payload box found to be  $2.0 \text{ G}$ .

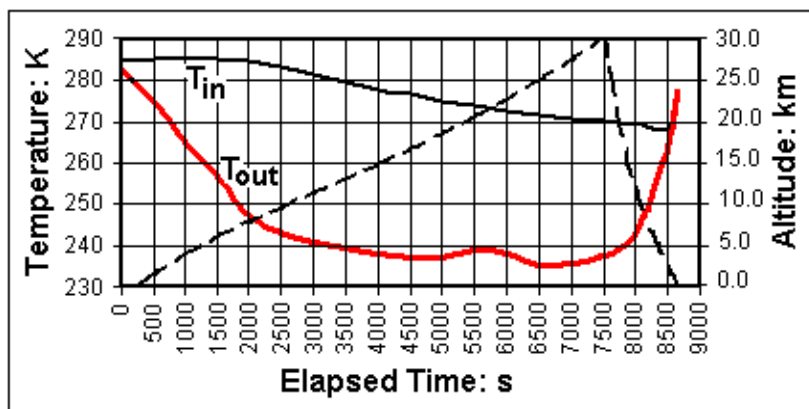


**Figure 8:** The temperatures recorded by the on board digital temperature sensors inside ( $T_{in}$ ) and outside ( $T_{out}$ ) of the payload box and balloon altitude as functions of elapsed time.

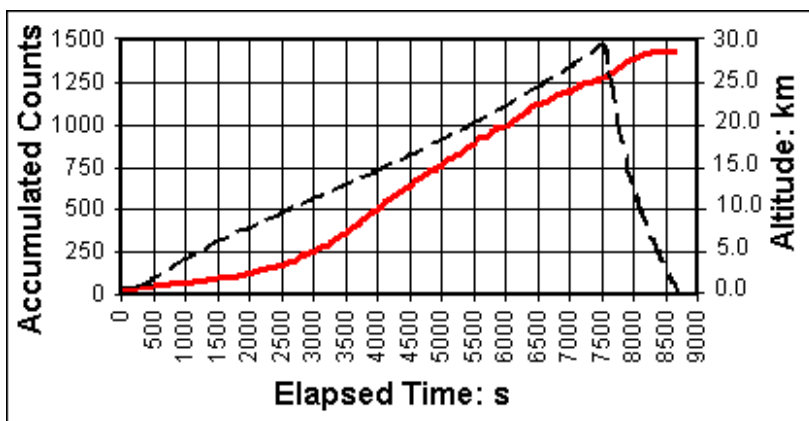


**Figure 9:** Accumulated cosmic ray photon counts sampled by SUGAR dosimeter every 10 seconds and balloon altitude are depicted as functions of elapsed time. Total accumulated counts during 8580 seconds balloon flight evaluated to be 1420.

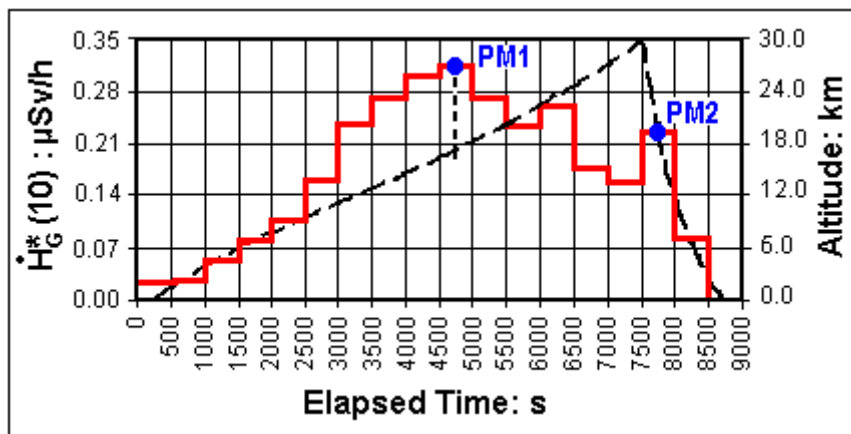


**Figure 10:** Showing the evaluated photon ambient dose equivalent rate  $\dot{H}_G^*(10)$  and balloon altitude as functions of elapsed time. High ambient dose equivalent rates were detected at long-lasting ascending (PM1) and very short descending (PM2) phases of Pfozter-Maximum.

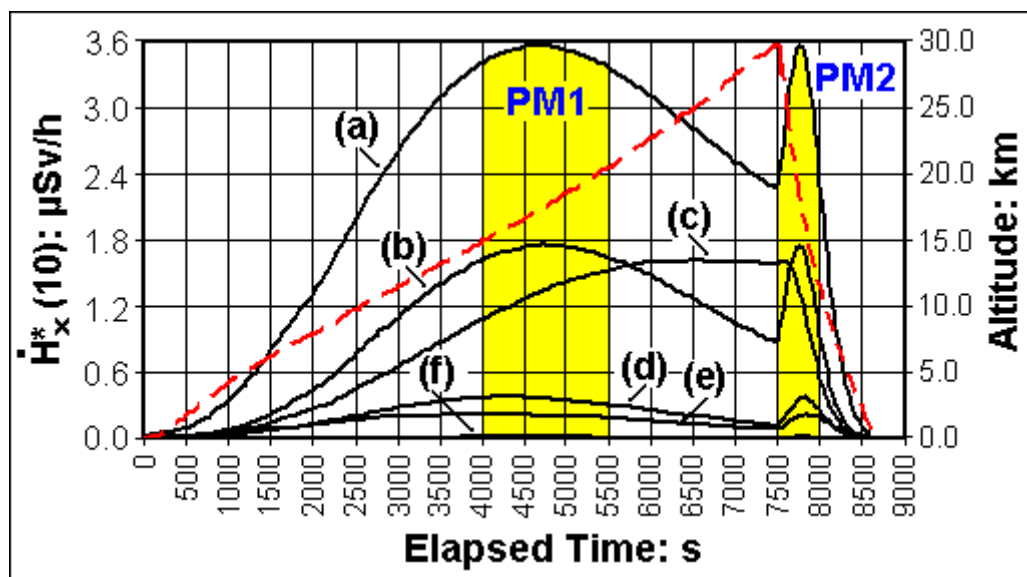


**Figure 11:** The ambient dose equivalent  $\dot{H}_x^*(10)$  rates of (a) neutrons, (b) electrons, (c) protons, (d) photons, (e) muons and (f) pions (too low to be visible in the graph) evaluated using modified EPCARD.Net code are plotted as functions of elapsed time (Table 3). The corresponding altitude profile is indicated by dotted line. The Pfozter-Maximums at ascending (PM1) and descending (PM2) phases are highlighted.

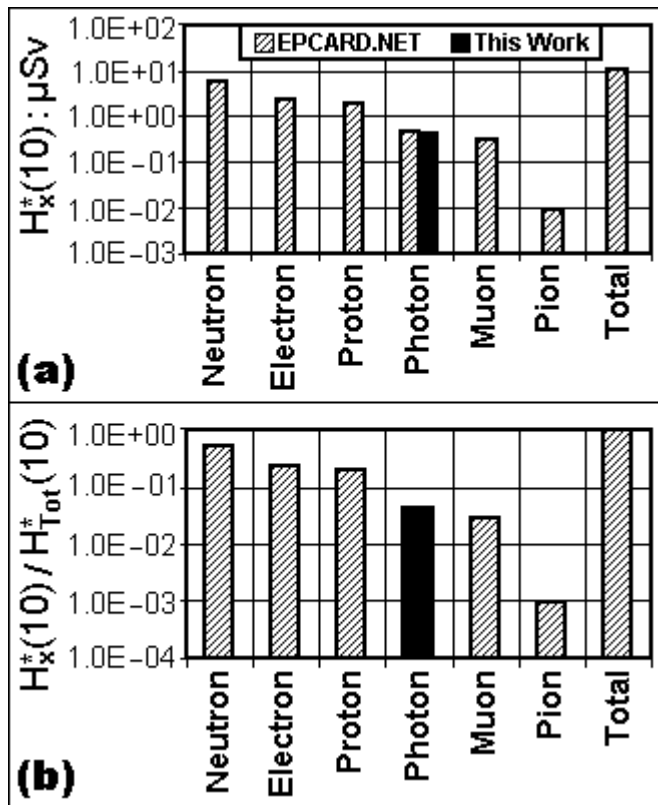


**Figure 12:** (a) Showing the neutron, photon, proton, electron, muon and pion ambient dose equivalents  $H_x^*(10)$  integrated over the balloon flight as calculated by EPCARD.Net code. The photon ambient dose equivalent  $H^*(10)$  recorded by SUGAR dosimeter (this work) is highlighted. (b) The contribution of ambient dose equivalent from individual cosmic ray components relative to total ambient dose equivalent  $H_x^*(10)/H_{\text{Tot}}^*(10)$ .

**Table 1:** Essential criteria of the ballooning mission subsystems (**Figure 1a**).

Subsystem	Criteria
Balloon	<i>Material:</i> Latex <i>Mass without payload:</i> 1.0 kg <i>Launch volume:</i> 4.2E+03 litre <i>Burst volume:</i> 2.7E+05 litre <i>Lifting gas:</i> Helium
Parachute	<i>Material:</i> Nylon <i>Mass:</i> 0.015 kg <i>Opening diameter:</i> 0.8 m
Payload Box	<i>Material:</i> Styrofoam <i>Thermal Conductivity:</i> 0.08 Wm <sup>-1</sup> K <sup>-1</sup> <i>Mass without payload:</i> 0.5 kg <i>Mass with payload:</i> 1.8 kg <i>Dimension:</i> 35 cm × 35 cm × 35 cm <i>Wall thickness:</i> 5 cm

**Table 2:** Attributes of the PIN-diode based SUGAR dosimeter (**Figure 3**).

Item/Attribute	Value/Test results
COTS radiation sensor	RD2014 (Module)
Total mass with PCB (Figure 3)	9.6 g
Footprint (Figure 3)	4.5 cm <sup>2</sup> (2.8 cm × 1.6 cm)
Operating voltage (measured)	5.0V
Current drain (measured)	2.9 mA
Power consumption	1.5 mW
<sup>60</sup> Co-Gamma calibration constant	5.8 (counts.min <sup>-1</sup> /μSv.h <sup>-1</sup> ) ± 15%
Gamma Energy Response	Constant within 1 - 100 MeV
Electron Energy Response	Immune to high-energy electrons
Temperature stability (243-333 K)	Guaranteed by the manufacturer
Vibration immunity (Balloon Flight)	Flawless operation up to 2.0G
Microwave (EMI) immunity	Guaranteed by the manufacturer

**Table 3:** Showing the ambient dose equivalent of cosmic ray components  $H_x^*(10)$  and their contribution (%) relative to total ambient dose equivalent  $H_{Tot}^*(10)$  of 10.66  $\mu\text{Sv}$ . These results include EPCARD.Net calculations and measurements using SUGAR dosimeter (this work). The standard deviations ( $1\sigma$ ) of EPCARD.Net calculations and SUGAR dosimeter measurements were  $\pm 20\%$  and  $\pm 15\%$  respectively.

Cosmic Radiation Components	Ambient Dose Equiv. $H_x^*(10)$ : $\mu\text{Sv}$		Rel. Contribution (%) $100 \times H_x^*(10)/H_{Tot}^*(10)$
	EPCARD.NET	This work	
Neutron	$5.52 \pm 1.1$	---	51.8
Electron	$2.31 \pm 0.46$	---	21.7
Proton	$2.04 \pm 0.41$	---	19.1
Photon	$0.47 \pm 0.09$	$0.36 \pm 0.05$	3.4
Muon	$0.31 \pm 0.06$	---	2.9
Pion	$0.01 \pm 0.002$	---	0.1
Total	10.66	---	100

## Figure and Table Captions

**Figure 1:** (a) The major subsystems of the ballooning mission including the balloon, payload box and parachute. (b) Screen-shot of the sky taken at high altitude; curvature of the earth is clearly visible. (c) Screen-shot of the balloon-burst took place at an altitude of 30 km, balloon fragments were flying apart and brightly illuminated by sunlight; whereas the sky in background remained pitch black.

**Figure 2:** Depicting the architecture of the balloon borne instrumentation board incorporating: Micro Controller Unit (MCU), 32 GB SD Card with reader (SDC), Watchdog with timer (WDT), 9V Lithium Polymer Battery (LPB), 900 MHz Ultra long range radio modem (TCV), Global Positioning System module (GPS), External temperature sensor (ET), Internal temperature sensor (IT), Digital accelerometer (AM), Gamma ray (SUGAR) dosimeter (GD) (Left) and a photograph of the prototype board (Right).

**Figure 3:** (a) Schematic diagram depicting the principle of PIN diode. (b) Schematic diagram of the SUGAR (Sydney University GAMMA Ray) dosimeter showing the PIN-Diode sensor module interfaced to pulse shaping circuit (PSC). (c) Cross section of the PIN diode dosimeter module highlighting the SiO<sub>2</sub> wafer, Electromagnetic Interference (EMI) shield and the energy compensation filter made of 0.2 mm thick Lead foil.

**Figure 4:** Photon mass energy absorption coefficients (Hubble and Seltzer, 1993) of commercial Lead ( $\rho = 11.34 \text{ gcm}^{-3}$ ) and SiO<sub>2</sub> ( $\rho = 2.32 \text{ gcm}^{-3}$ ) are plotted as functions of photon energy.

**Figure 5:** Output pulse train from SUGAR dosimeter recorded with a digital storage oscilloscope corresponds to a pulse height and a width of 3.8 V (TTL) and 10 ms respectively during <sup>60</sup>Co irradiation.

**Figure 6:** Showing the GPS ground trace of the balloon flight. The traversed distance between the launching (West Wyalong) and landing (Weddin Mountains National Park) locations was 66.2 km.

**Figure 7:** Acceleration (vibration) profile recorded by on board digital accelerometer and balloon altitude as functions of elapsed time. The average ascending rate of the balloon and the descending rate of the payload box were calculated to be 4.0 and 25.0 ms<sup>-1</sup>, respectively. The maximum acceleration (vibration) endured by the payload box found to be 2.0 G.

**Figure 8:** The temperatures recorded by the on board digital temperature sensors inside ( $T_{in}$ ) and outside ( $T_{out}$ ) of the payload box and balloon altitude as functions of elapsed time.

**Figure 9:** Accumulated cosmic ray photon counts sampled by SUGAR dosimeter every 10 seconds and balloon altitude are depicted as functions of elapsed time. Total accumulated counts during 8580 seconds balloon flight evaluated to be 1420.

**Figure 10:** Showing the evaluated photon ambient dose equivalent rate  $\dot{H}_G^*(10)$  and balloon altitude as functions of elapsed time. High ambient dose equivalent rates were detected at long-lasting ascending (PM1) and very short descending (PM2) phases of Pfozter-Maximum.

**Figure 11:** The ambient dose equivalent  $\dot{H}_x^*(10)$  rates of (a) neutrons, (b) electrons, (c) protons, (d) photons, (e) muons and (f) pions (too low to be visible in the graph) evaluated using modified EPCARD.Net code are plotted as functions of elapsed time (Table 3). The corresponding altitude profile is indicated by dotted line. The Pfozter-Maximums at ascending (PM1) and descending (PM2) phases are highlighted.

**Figure 12:** (a) Showing the neutron, photon, proton, electron, muon and pion ambient dose equivalents  $H_x^*(10)$  integrated over the balloon flight as calculated by EPCARD.Net code. The photon ambient dose equivalent  $H^*(10)$  recorded by SUGAR dosimeter (this work) is highlighted. (b) The contribution of ambient dose equivalent from individual cosmic ray components relative to total ambient dose equivalent  $H_x^*(10)/H_{Tot}^*(10)$ .

**Table 1:** Essential criteria of the ballooning mission subsystems (**Figure 1a**).

**Table 2:** Attributes of the PIN diode based SUGAR dosimeter (**Figure 3**).

**Table 3:** Showing the ambient dose equivalent of cosmic ray components  $H_x^*(10)$  and their contribution (%) relative to total ambient dose equivalent  $H_{Tot}^*(10)$  of 10.66  $\mu$ Sv. These results include EPCARD.Net calculations and measurements using SUGAR dosimeter (this work). The standard deviations ( $1\sigma$ ) of EPCARD.Net calculations and SUGAR dosimeter measurements were  $\pm 20\%$  and  $\pm 15\%$  respectively.